

Correlation between Line Width and Line Flux of Double-Peaked Broad $H\alpha$ of 3C390.3

Xue-Guang Zhang^{1,2*}

¹Purple Mountain Observatory, Chinese Academy of Sciences, 2 Beijing XiLu, NanJing, JiangSu, 210008, P. R. China

²Chinese Center for Antarctic Astronomy, NanJing, JiangSu, 210008, P. R. China

ABSTRACT

In this manuscript, we carefully check the correlation between the line width (second moment) and the line flux of the double-peaked broad $H\alpha$ of the well-known mapped AGN 3C390.3, in order to show some further distinctions between double-peaked emitters and normal broad line AGN. Based on the Virialization assumption $M_{BH} \propto R_{BLR} \times V^2(BLR)$ and the empirical relation $R_{BLR} \propto L^{\sim 0.5}$, one strong negative correlation between the line width and the line flux of the double-peaked broad lines should be expected for 3C390.3, such as the negative correlation confirmed for the mapped broad line object NGC5548, $R_{BLR} \times V^2(BLR) \propto L^{\sim 0.5} \times \sigma^2 = constant$. But, based on the public spectra around 1995 from the AGNWATCH project for 3C390.3, one reliable positive correlation is found between the line width and the line flux of the double-peaked broad $H\alpha$. In the context of the proposed theoretical accretion disk model for double-peaked emitters, the unexpected positive correlation can be naturally explained, due to different time delays for inner parts and outer parts of disk-like BLR of 3C390.3. Moreover, the Virialization assumption is checked and found to be still available for 3C390.3. However, time-varying size of the BLR of 3C390.3 can not be expected by the empirical relation $R_{BLR} \propto L^{\sim 0.5}$. In other words, the mean size of BLR of 3C390.3 can be estimated by the continuum luminosity (line luminosity), while, the continuum emission strengthening leads to the size of BLR decreasing (not increasing) in different moments for 3C390.3. Then, we compared our results of 3C390.3 with the previous results reported in the literature for the other double-peaked emitters, and found that before to clearly correct effects from disk physical parameters varying (such as effects of disk precession) for long-term observed line spectra, it is not so meaningful to discuss the correlation of line parameters of double-peaked broad lines. Furthermore, due to the probable 'external' ionizing source with so far unclear structures, it is hard to give one conclusion that the positive correlation between the line width and the line flux can be found for all double-peaked emitters, even after the considerations of disk physical parameters varying. However, once one positive correlation of broad line parameters was found, the accretion disk origination of the broad line should be firstly considered.

Key words: Galaxies:Active – Galaxies:nuclei – Galaxies:Seyfert – quasars:Emission lines – Galaxies:individual: 3C390.3

1 INTRODUCTION

As one well-known double-peaked emitter (AGN with double-peaked broad low-ionization emission lines), 3C390.3 has been studied for more than two decades, since clear double-peaked broad balmer lines were reported by Burbidge & Burbidge (1971, spectrogram of 3C390.3) and by Perez et al. (1988, clear spectral lines). Based on double-peaked appearance of the broad lines and characters of long-

term variabilities of the broad lines and continuum emission, among those proposed theoretical models for double-peaked emitters (such as binary black hole model: Begelman et al. 1980, Boroson & Lauer 2009, Gaskell 1996, Lauer & Boroson 2009, Zhang et al. 2007, double stream model: Vellieux & Zheng 1991, Zheng et al. 1990, 1991, accretion disk model: Bachev 1999, Chen et al. 1989, Chen & Halpern 1989, Chornock et al. 2010, Eracleous et al. 1995, Flohic & Eracleous 2008, Gaskell 2010, Gezari et al. 2007, Hartnoll & Blackman 2000, 2002, Karas et al. 2001, Lewis et al. 2010, Oke 1987, Perez et al. 1988, Storchi-Bergmann, et al., 2003,

* xgzhang@pmo.ac.cn

Schimoia et al. 2012, Tran 2010), the accretion disk model (double-peaked broad lines coming from central accretion disk) has been widely accepted for the double-peaked emitter 3C390.3 (Chen et al. 1989, Chen & Halpern 1989, Dietrich et al. 2012, Eracleous et al. 1997, Livio & Xu 1997, Oke 1987, Perez et al. 1988, Popovic et al. 2011, Shapovalova et al. 2001, 2010, Zhang 2011a). Then based on the proposed theoretical accretion disk model, besides the different line profiles, we try to find some interesting distinctions between the double-peaked emitter 3C390.3 and normal broad line AGN, which is the main objective of our manuscript.

As we commonly know that motions of broad emission line clouds in BLR (broad emission line regions) of AGN are gravitationally dominated by central mass of AGN (Gaskell 1988, 1996, Krause et al. 2011, Kollatschny & Zetzl 2011, Netzer & Marziani 2010, Peterson & Wandel 1999, Wandel et al. 1999, and references therein), which provides strong evidence for applying Virialization assumption to estimate virial black hole masses of broad line AGN (Bennert et al. 2011, Collin et al. 2006, Greene & Ho 2004, 2005, Kelly & Bechtold 2007, Marziani et al. 2003, Netzer & Marziani 2010, Onken et al. 2004, Park et al. 2012, Peterson et al. 2004, Peterson 2010, Rafiee & Hall 2011, Shen & Liu 2012, Sulentic et al., 2000, Vestergaard 2002, Wu et al. 2004). Then based on the Virialization assumption, combining with widely accepted empirical relation to estimate size of BLR of AGN ($R_{BLR} \propto L^{0.5}$, Bentz et al. 2006, 2009, Denney et al. 2010, Kaspi et al. 1996, 2000, 2005, Greene et al. 2010, Wang & Zhang 2003), we will have

$$M_{BH} \propto R_{BLR} \times V(BLR)^2 \propto L(H\alpha_B)^{0.5} \times V^2(H\alpha_B) \quad (1)$$

where index $H\alpha_B$ means corresponding line parameters of broad $H\alpha$. Moreover, we can find that for individual object ($M_{BH} = constant$ and $L(H\alpha_B) \propto flux(H\alpha_B)$),

$$\begin{aligned} L(H\alpha_B) \times V(H\alpha_B)^4 &= constant \\ flux(H\alpha_B) \times V(H\alpha_B)^4 &= constant \\ L(H\alpha_B)(or R_{BLR} or flux(H\alpha_B)) \uparrow &\implies V(H\alpha_B) \downarrow \end{aligned} \quad (2)$$

In other words, line width of broad emission lines is decreasing with line luminosity (size of BLR, continuum luminosity) increasing. The strong expected negative correlation, R_{BLR} versus V , have been found and reported for several well mapped objects, such as NGC5548 (Bentz et al. 2007, Denney et al. 2010, Peterson et al. 2002, 2004, Wanders & Peterson 1996), NGC3783 and NGC7469 (Peterson et al. 2004), Arp151 (Park et al. 2012). Certainly, the correlation between R_{BLR} and V for 3C390.3 is also shown in Peterson et al. (2004), however, there is no one reliable correlation confirmed for 3C390.3, due to the less number of data points (only 4 data points for 3C390.3 shown in Figure 8 in Peterson et al. 2004). In the paper, we will carefully re-check the correlation for 3c390.3, because among the well-mapped objects, 3c390.3 is the unique double-peaked emitter.

In the paper, we check correlation between line width and line flux, rather than to check correlation between size of BLR and line width, in order to obtain abundant data points. This paper is organized as follows. Section 2 gives our data procedures and main results. Section 3 shows our discussions and conclusions. Here, cosmological parameters

$H_0 = 70 \text{ km} \cdot \text{s}^{-1} \text{ Mpc}^{-1}$, $\Omega_\Lambda = 0.7$ and $\Omega_m = 0.3$ have been adopted.

2 MAIN RESULTS

All public spectra of 3C390.3 can be collected from the AGNWATCH project (<http://www.astronomy.ohio-state.edu/~agnwatch/>), which is a consortium of astronomers who have studied the inner structures of AGN through continuum and emission-line variability. Detailed descriptions about observational instruments, techniques and procedures to reduce the spectra of 3C390.3 can be found in Dietrich et al. (1998), which will not be described any more. Here, we mainly show our procedures to measure line parameters (line width and line flux) of the double-peaked broad lines of 3C390.3, and show our results about correlation of the line parameters.

2.1 Line Parameters

We mainly focus on line parameters of broad $H\alpha$ of 3C390.3, due to the following two main reasons. On the one hand, the broad $H\alpha$ is much stronger than the broad $H\beta$, which leads to more reliable line parameters. On the other hand, there is much less contamination on the broad $H\alpha$. Only the narrow emission lines, the narrow $H\alpha$ and [N II] doublet, have effects on the measured line parameters of the double-peaked broad $H\alpha$. However, for the double-peaked broad $H\beta$, besides the common narrow $H\beta$ and [O III] doublet, the extended [O III] doublet and some weak optical Fe II emission lines (Dietrich et al. 2012) have effects on the measured line parameters of the broad $H\beta$. Thus, focusing on the observed spectrum around $H\alpha$ of 3C390.3 should lead to more accurate line parameters and to find more reliable correlation of the line parameters.

For 3C390.3, there are 67 public spectra observed around 1995 including available $H\alpha$ which can be collected from the AGNWATCH project, based on those reported parameters listed in Table 9 in Dietrich et al. (1998). Then the line parameters of the double-peaked broad $H\alpha$ are measured as follows. In order to ignore effects of the narrow lines, the double-peaked broad component of $H\alpha$ is firstly described and fitted by the theoretical elliptical accretion disk model proposed by Eracleous et al. (1995). Here, our main objective is not to accurately determine the disk parameters through theoretical model, thus, there are no further discussions about disk parameters, which has been discussed in detail in our another paper (Zhang 2011a, Paper I). In other words, we only require that the line profiles of the double-peaked broad $H\alpha$ can be best described and be well separated from the narrow lines. In this paper, we show the best fitted results for the apparent double-peaked broad $H\alpha$ in Figure 1, and the corresponding residuals in Figure 2. In Figure 2, we also show the best fitted results for the narrow lines of $H\alpha$ and [N II] λ 6548, 6583Å by three standard gaussian functions with the same redshift and with line parameters ratio of [N II] doublet fixed to theoretical values. Based on the results shown in Figure 1 and Figure 2, the double-peaked broad component of $H\alpha$ can be clearly separated from the narrow lines.

Then, the line width (second moment) and the line flux

of the double-peaked broad component can be estimated by (Peterson et al. 2004)

$$\sigma_{H\alpha}^2 = \frac{\int_{\lambda} \lambda^2 \times P_{\lambda} d\lambda}{\int_{\lambda} P_{\lambda} d\lambda} - \left(\frac{\int_{\lambda} \lambda \times P_{\lambda} d\lambda}{\int_{\lambda} P_{\lambda} d\lambda} \right)^2 \quad (3)$$

$$flux(H\alpha) = \int_{\lambda} P_{\lambda} d\lambda$$

where P_{λ} is the line profile of the double-peaked broad $H\alpha$ after subtraction of the narrow lines. Here, the main reasons to use the second moment rather than FWHM (full width at half maximum) are: the second moment rather than the FWHM can be used to well trace Kepler velocities of broad line clouds in BLR of AGN (Fromerth & Melia 2000, Peterson et al. 2004), the second moment rather than the FWHM is well defined for arbitrary line profiles (such as the double-peaked broad line profile), and moreover the second moment rather than the FWHM has relatively lower uncertainty (Peterson et al. 2004). The measured line widths (σ) of the double-peaked broad $H\alpha$ from the observed spectra are listed in Table 1.

Before proceeding further, it is necessary to estimate the corresponding uncertainty of the measured line width of the double-peaked broad $H\alpha$. Here, the commonly used bootstrap method (Peterson et al. 1998, 2004, Press et al. 1992, Zhang 2011b) is applied to estimate the uncertainty. Based on each observed double-peaked broad $H\alpha$ with narrow lines ([N II], [S II], [O I] doublets and narrow $H\alpha$) having been subtracted, 400 mock double-peaked lines can be created by the bootstrap method. When the bootstrap method is applied, we should avoid the selection of some adjacent data points to create mock lines, otherwise, the following estimated uncertainty should be unreasonably small, due to few variation of line profile. Then line widths of the 400 mock lines are measured by Equation (3). After that, standard deviation of the 400 measured line widths of the mock lines is accepted as the uncertainty of the line width of the observed double-peaked broad $H\alpha$, and listed in Table 1. Certainly, we should note that Peterson et al. (2004) accepted $\sigma_{err}/\sigma = 81\text{km/s}/3185\text{km/s} \sim 2.5\%$ as the mean uncertainty of the line width of broad $H\beta$ of 3C390.3 within observed wavelength range from 5006Å to 5246Å. It is consistent with our value $\langle \sigma_{err}/\sigma \rangle \sim 2.2\%$, which indicates our estimated uncertainties for the line width of all the 67 double-peaked broad $H\alpha$ are reasonable and acceptable.

Besides the line width and the corresponding uncertainty, it is not difficult to accomplish spectral flux calibration for 3C390.3. However, because the spectra of 3C390.3 are observed by different instruments in different observatories under different configurations, the flux calibration based on the direct observed line profile should have low confidence level. As discussed in detail in the section 2 of Dietrich et al. (1998), some further procedures have been applied to complete the flux calibration. The spectra are firstly photometrically calibrated by comparison with the broadband photometric measurements (being convolved with the spectral response curve of the Johnson V and R), and then scaled by multiplicative factors to achieve the same total flux ratio as the intercalibrated photometric measurements in V and R bands. After that, the spectra have to be intercalibrated to a common flux level, in order to correct the effects for different wavelength shifts, and different spectral resolutions in different spectra. All the procedures have been successfully

done by Dietrich et al. (1998), so that we directly collect the line fluxes (f_1) and corresponding uncertainties of broad $H\alpha$ listed in Dietrich et al. (1998). Moreover, in spite of the effects from different flux scales for the observed spectra, those directly measured line fluxes of the double-peaked broad $H\alpha$ (f_0 , no corrections being considered) are also listed in Table 1.

Before the end of the subsection, there are two points we should note. On the one hand, we do not try to confirm that the pure elliptical accretion disk model (Eracleous et al. 1995) is the unique true physical model for the double-peaked emitter 3C390.3. We only use the theoretical disk model to separate the double-peaked broad component from the narrow lines. The properties of the residuals shown in Figure 2 for the best fitted results shown in Figure 1 illustrate that it is one good choice to determine the double-peaked broad component by the theoretical elliptical disk model for the spectra around 1995. On the other hand, although we do not apply the intercalibration method (Van Groningen & Wanders 1992) to correct the effects from small wavelength shifts, different spectral resolutions and different flux scales for different spectra as what have been done in Dietrich et al. (1998), the measured second moment through observed spectrum is accurate and reliable, because the applied broadening velocity in the intercalibration method for 3C390.3 is only ten or more kilometers per second or smaller, which is can be totally ignored for the measured second moment and the corresponding uncertainty of the double-peaked broad $H\alpha$. Thus, the following results based on the measured second moments are reliable.

2.2 On correlation between the line width and the line flux of the double-peaked broad $H\alpha$

Figure 3 shows the correlation between the line width and the line flux of the double-peaked broad $H\alpha$ of 3C390.3. Linear correlation coefficient for the correlation of f_0 versus σ is about 0.28 with two-sided significance of deviation from zero about $P_{null} \sim 0.04$ for all the 67 spectra listed in Table 1. The coefficient for the correlation of f_1 (accurate line flux of $H\alpha$ from the AGNWATCH project) versus σ is about 0.45 with $P_{null} \sim 0.0002$. It is clear that there is one positive correlation between the line width and the line flux of the double-peaked broad $H\alpha$ for 3C390.3. Furthermore, under considerations of the uncertainties of the parameters in both coordinates, the best fitted results for f_1 versus σ can be written as

$$\frac{\sigma}{\text{\AA}} \propto (0.065 \pm 0.006) \times \frac{f_1}{10^{-16}\text{erg/s/cm}^2} \quad (4)$$

Certainly, we should note the accurate flux f_1 collected from the AGNWATCH project includes the contributions from the narrow emission lines of $H\alpha$ and [N II] doublet. However, the contributions do not affect the positive correlation, because the flux of the narrow emission lines of each spectrum is constant. The best fitted results are shown as solid lines in Figure 3. The corresponding 99.95% confidence bands for the best fitted results are also shown in Figure 3.

It is clear that the uncertainty of the measured second moment (σ_{err}) of the double-peaked broad $H\alpha$ has important effects on our final conclusion about the positive correlation for 3C390.3, because the varying range of second

moment is not large, $\sim 90\text{\AA} < \sigma < \sim 100\text{\AA}$. If the uncertainty of the second moment is large enough to cover the varying range of the second moment, the shown positive correlation in Figure 3 should be fake. Thus, it is necessary to check whether larger uncertainties should be possible for our measured line width. Here, we simply consider the question as follows. For one given theoretical line profile of the double-peaked broad H α with second moment σ (solid line shown in Figure 1) best fitted for the observed line profile, if the corresponding uncertainty σ_{err} for the second moment is reasonable, we will find that after being broadened by velocity σ_b for the theoretical line profile, the new theoretical line profile with second moment $\sigma_{new} = \sigma + \sigma_{err}$ still well describes the observed double-peaked broad line profile of H α . Here, the value of σ_b can be determined by $\sigma_b^2 = \sigma_{new}^2 - \sigma^2$. Based on the listed values in Table 1, we can find that the common broadening velocity is around 20\AA ($\sim 1000\text{km/s}$). Figure 4 shows one example about the being broadened line profile. In the figure, we can find that the being broadened line profile (the IDL function 'convol' being applied) with $\sigma_b = 1000\text{km/s}$ has begun to lead to some bad fitted results for the spectrum around the blue peak ($\sim 6500\text{\AA}$) of the double-peaked broad H α , which indicates larger broadening velocity should be unreasonable. In other words, the varying range of the second moment is larger enough to ignore the effects of the uncertainty of the second moment on the positive correlation shown in Figure 3, and the positive correlation is reliable.

Besides the unexpected positive correlation shown in Figure 3 for 3C390.3, we wish to check the correlation of line parameters of broad lines for the other well-known mapped normal broad line AGN, in order to frankly show that the positive correlation for the double-peaked emitter 3C390.3 is very interesting. There are more than 40 nearby mapped objects reported in the literature (Barth et al. 2011, Bentz et al. 2006, 2009, 2010, Denney et al. 2006, 2009, 2010, kaspil et al. 1996, 2000, 2005, 2007, Peterson et al. 2004). The simple correlation between the BLR size and the line width for part of those objects can be found in the corresponding literatures. Here, NGC5548 is selected as our target, because there is one well sample of fine spectra with homogeneous high-quality for NGC5548 (Bentz et al. 2007, Dietrich et al. 1993, Korista et al. 1995, Peterson et al. 1991, 1992, 1994, 1999, 2002, 2004, Popovic et al. 2008, Sergeev et al. 2007, Shapovalova et al. 2004, Wanders & Peterson 1996). Some detailed information about the spectra of NGC5548 can be found in the website of the AGNWATCH project. Here, we mainly focus on the spectra studied in detail in Wanders & Peterson (1996) and collect the spectra with necessary corrections having been done by Wanders & Peterson, i.e., the collected 247 spectra have been scaled through the van Groningen-Wanders method, and have the underlying continuum subtracted, and have the narrow components removed as well, and no further corrections are necessary for the following measured line parameters. Then based on the collected 247 spectra of NGC5548 observed from Dec. 1988 to Sep. 1993., the line width and the line flux can be easily determined by Equation (3), within observed wavelength range from 4840\AA to 5030\AA . Then, uncertainty of the line flux is determined by uncertainty in spectral flux provided by the AGNWATCH project, and uncertainty of the line width is determined by the bootstrap method. Here, we do

not show all the observed spectra of NGC5548, but only show one spectrum as an example in the top-right panel of Figure 5. The measured line parameters and corresponding uncertainties of the broad H β of NGC5548 are listed in Table 2.

Figure 5 shows the correlation between the line width and the line flux of the broad H β for NGC5548. The linear correlation coefficient is about -0.83 with $P_{null} \sim 0$. The best fitted results with the considerations of the uncertainties of the parameters in both coordinates can be written as

$$\log\left(\frac{\text{flux}(H\beta)}{10^{-14}\text{erg/s/cm}^2}\right) \propto (-4.25 \pm 0.11) \times \log\left(\frac{\sigma(H\beta)}{\text{\AA}}\right) \quad (5)$$

It is clear there is one strong negative correlation for NGC5548, which is well consistent with the expected result under the Virialization assumption: $L(H\beta_B) \propto \sigma(H\beta_B)^{-4}$. Undoubtedly, the negative correlation is well consistent with the negative correlation between the size of BLR and the line width found in Bentz et al. (2006), Denney et al. (2010) and Peterson et al. (2004).

Based on the results above, we can find that there is one reliable positive correlation between the line width and the line flux of the double-peaked broad H α for the double-peaked emitter 3C390.3, which is against the expected negative correlation confirmed for the other mapped AGN. The unexpected positive correlation should indicate different structures of BLRs of the double-peaked emitter 3C390.3 and normal broad line AGN.

3 DISCUSSIONS AND CONCLUSIONS

It is clear that the reliable positive correlation shown in Figure 3 for the double-peaked emitter 3C390.3 is against the expected result through the Virialization assumption. Thus the following three questions are mainly considered, what determines the unexpected positive correlation? whether the Virialization assumption is still available for double-peaked emitters? whether the unexpected positive correlation can be found for the other double-peaked emitters?

3.1 Accretion Disk Model for Double-Peaked Emitters

For normal broad line AGN, such as NGC5548, the strong negative correlation of the broad line parameters can be naturally explained by the following simple viewpoint: BLR kinematics are dominated by central gravity (some more recent reviews can be found in Down et al. 2010, Sluse et al. 2011), which could be well appropriate to the broad line Seyfert 1 galaxy NGC5548 (Bentz et al. 2007, Denney et al. 2010, Peterson et al. 2002, 2004, Wanders & Peterson 1996,) and some other mapped broad line AGN (Peterson et al. 2004): stronger continuum emission leads to deeper ionization boundary (larger flux-weighted size of BLR) and leads to smaller general rotating velocity (smaller line width). And then, through the broad line strength being applied to estimate the size of BLR, $R_{BLR} \propto L(H\alpha)^{\sim 0.5}$, the negative correlation of the line width and the line flux can be found. Certainly, the viewpoint is not appropriate to the double-peaked emitter 3C390.3.

If the theoretical accretion disk model was accepted,

what result about the correlation between the size of BLR and the continuum/line flux should be expected for 3C390.3? In the context of the theoretical disk model for double-peaked emitters, such as the elliptical accretion disk model (Eracleous et al. 1995) which can be well applied to best fit the observed line spectra of 3C390.3 observed around 1995, the disk-like BLR is locating into the central accretion disk, and does share the kinematic characters of the central accretion disk. For 3C390.3, the inner and outer boundary radii of the elliptical disk-like BLR are about $R_{in} \sim 150 - 250R_G$ and $R_{out} \sim 1100 - 1400R_G$, under the theoretical accretion disk model (Eracleous & Halpern 1994, 2003, Flohic & Eracleous 2008, Shapovalova et al. 2001, Zhang 2011a, Paper I). Based on the oversimplified extended disk-like BLR (no considerations of tiny contributions from probable hot spots, warped structures, spiral arms etc. for 3C390.3 around 1995), one simple result can be expected: stronger continuum emission leads to stronger broad line emission coming from the inner part of the disk-like BLR (and then larger line width) in one short period (much shorter than the traveling time for ionizing photons through the whole BLR), because the stronger ionizing continuum firstly reaches the inner part of the disk-like BLR.

In other words, stronger continuum emission (strong line flux) leads to larger flux ratio of the broad $H\alpha$ from the inner part of the BLR to the broad $H\alpha$ from the outer part of the BLR, and leads to larger line width due to larger contributions from the higher velocity clouds in inner part of BLR, which is similar as the results shown in Figure 3. So that, we check the properties of the broad line flux ratio $R = f_{1/2}/f_{all}$, where $f_{1/2}$ means the broad line flux coming from the inner part of disk-like BLR with radius from R_{in} to $0.5 \times (R_{in} + R_{out})$ and f_{all} means the measured total broad line flux. The calculated value of R for each spectrum is listed in Table 1. Figure 6 shows the correlation between the line flux f_0 (f_1) and the parameter of R . In the figure, the shown uncertainty of R is determined by the uncertainty of f_1 collected from the AGNWATCH project. The spearman-rank correlation coefficient for the correlation is about 0.49 with $P_{null} \sim 10^{-5}$ for the parameter f_1 in Table 1 and 0.26 with $P_{null} \sim 4\%$ for the parameter f_0 in Table 1. The positive correlation in Figure 6 indicates the proposed disk origination for the double-peaked broad $H\alpha$ of 3C390.3 can be naturally applied to explain the unexpected positive correlation shown in Figure 3.

Moreover, if the observed broad $H\alpha$ of 3C390.3 was separated into two parts: one part with larger line width (σ_1) coming from the inner region of the disk-like BLR with radius from R_{in} to $0.5 \times (R_{in} + R_{out})$, and the other part with smaller line width (σ_2) coming from the outer region of the disk-like BLR, then the line width (σ) of the total observed double-peaked broad $H\alpha$ can be re-written as (Zhang 2011b)

$$\sigma^2 = R \times \sigma_1^2 + (1 - R) \times \sigma_2^2 \quad (6)$$

where R is the flux ratio of $R = f_{1/2}/f_{all}$. The equation above can be easily proved by definition of second moment (Equation 3). Based on the mean disk parameters shown in our paper I (Zhang 2011a), we have $\sigma_1 \sim 109\text{\AA}$ and $\sigma_2 \sim 69\text{\AA}$. Through the equation above, in order to obtain the measured line width of the double-peaked broad $H\alpha$ varying from $\sim 92\text{\AA}$ to $\sim 100\text{\AA}$ (minimum and maximum values for

the second moment of broad $H\alpha$ of 3C390.3), the parameter of R should be varying from ~ 0.53 to ~ 0.73 , which is consistent with the shown results about R in Figure 6 and in Table 1.

The results above indicate that the unexpected positive correlation shown in Figure 3 for 3C390.3 can be naturally explained by the proposed accretion disk origination of the double-peaked broad $H\alpha$. Certainly, here we do not consider effects from probable 'external' ionizing source for the double-peaked emitter 3C390.3, which will be discussed in detail in subsection 3.4.

3.2 Virialization Assumption

As the most convenient method to estimate central black hole masses of broad line AGN, the virialization assumption has been widely and commonly accepted. Here, we should find that the assumption is also valid for the double-peaked emitter 3C390.3.

As we have shown above, the proposed accretion disk model should be appropriate for the double-peaked emitter 3C390.3. Considering the oversimplified case, the disk-like BLR of 3C390.3 is separated into one inner region with radius from R_{in} to $0.5 \times (R_{in} + R_{out})$ and the other outer region, then the flux weighted distance between the two regions to the central black hole can be calculated based on the simple elliptical accretion disk model (Eracleous et al. 1995) $R_{BLR,1} \sim 445R_G$ for the inner part of the BLR and $R_{BLR,2} \sim 987R_G$ for the outer part of the BLR. According to the results shown in Zhang (2011b), the size of total BLR (R_{BLR}) can be written as

$$R_{BLR} = R \times R_{BLR,1} + (1 - R) \times R_{BLR,2} \quad (7)$$

Based on the values of R listed in Table 1 and the values of $R_{BLR,1}$ and $R_{BLR,2}$, we will have the size of BLR R_{BLR} varying from $\sim 596R_G$ to $\sim 715R_G$. Moreover, based on the Virialization assumption, $R_{BLR} \times \sigma^2 = constant$ (or $(\frac{\sigma_{max}}{\sigma_{min}})^2 = \frac{R_{BLR,max}}{R_{BLR,min}}$), combining with the measured line width in Table 1, the expected maximum variation of the size of BLR of 3C390.3 calculated through the variations of the line width should be $(\frac{\sigma_{max}}{\sigma_{min}})^2 = (\frac{\sim 100\text{\AA}}{\sim 92\text{\AA}})^2 \sim 1.18$, which is consistent with the results above $\frac{R_{BLR,max} \sim 715R_G}{R_{BLR,min} \sim 596R_G} \sim 1.19$.

The results above indicate that the virialization assumption is still available for the double-peaked emitter 3C390.3. However, the common empirical relation $R_{BLR} \propto L^{\sim 0.5}$ is not available to show the properties of **time-varying** size of BLRs of 3C390.3. In other words, based on the **mean** continuum luminosity (broad line luminosity) in one long period, the **mean** size of BLR can be estimated by the empirical relation $R_{BLR} \propto L^{\sim 0.5}$, however, the time-varying size of BLR is decreasing with the line luminosity increasing.

3.3 Previous Results

Besides the well-known double-peaked emitter 3C390.3, there are several other double-peaked emitters, of which the double-peaked broad line profiles have been studied and reported. Some simple results about correlation between peak separation (in some literature, peak separation was used as

substitute for line width) and line flux (continuum emission) can be found.

In Figure 4 of Shapovalova et al. (2001), we can find one rough negative correlation between peak separation and line flux (continuum emission) for the double-peaked broad $H\beta$ of 3C390.3 observed from 1995 to 2000. Similarly negative correlation can be found for the double-peaked broad $H\alpha$ of NGC1097 (Schimoia et al. 2012, Storchi-Bergmann et al. 2003). However, through study of one sample of double-peaked emitters, Lewis et al. (2010) have shown that there is no confirmed correlation between the peak separation and the line flux for long-term observed double-peaked broad $H\alpha$, and additionally, the expected negative correlation between the line width (either FWHM or FWQM) and the broad $H\alpha$ flux is not observed. The contradictory is mainly due to the following reason: there are important effects on peak separation from varying of physical disk parameters, such as the effects from accretion disk precession, in the context of the accretion disk model for double-peaked emitters.

As we have seen that the proposed accretion disk models for double-peaked emitters lead to one important result: disk precession (or physical disk structure parameters varying) dominates the line profile variations of double-peaked broad line, besides the not so important contributions from the other subtle structures, such as the hot spots, warped structures etc.. In some cases, such as disk-like BLR with large eccentricity $e \sim 0.4$ under the elliptical accretion disk model, even there were no variations of continuum emission, only the orientation angle of elliptical rings ϕ_0 varying (pure accretion disk precession) should lead line width (second moment) varying by 30%, which can be simply verified by the proposed theoretical models. Thus, when we consider the correlation of the line parameters of double-peaked broad lines, the effects from the accretion disk precession (or from the other physical disk parameters varying) should be firstly corrected. However, before confirming one clear theoretical model for one double-peaked emitter, it is hard to correct these effects. One good choice to ignore the effects of accretion disk parameters varying is to consider short-term observed spectra with few variations of line profiles. That is the main reason why only the spectra around 1995 are collected for the double-peaked emitter 3C390.3, because the line profiles around 1995 are almost stable with less effects from disk parameters varying, as what we have discussed in our Paper I (Zhang 2001a). However, in Lewis et al. (2010), Schimoia et al. (2012), Shapovalova et al. (2001) and Storchi-Bergmann et al. (2003), the observed double-peaked broad lines have apparent variations of both peak flux ratios and peak positions, which indicate apparent variations of accretion disk physical parameters. If only continuum variations are considered, there should be much weak variations for peak positions and peak flux ratios, besides apparent variations of line intensity.

Moreover, We further check the listed parameters in the literature for the double-peaked emitter 3C390.3, under the virialization assumption: $R_{BLR} \times V^2(BLR) = constant$. In Wandel et al. (1999) and Peterson et al. (2004), the size of BLR and the corresponding line width are $R_{BLR,2004} \sim 24 \pm 6 \text{light} - \text{days}$ and $FWHM(2004) \sim 10000 \text{km/s}$ for 3C390.3 around 1995. In Shapovalova et al. (2001), the size of BLR and the corresponding line width are $R_{BLR,2001} \sim$

$90 \pm 10 \text{light} - \text{days}$ (similar results can be found in Popovic et al. 2011, some larger results can be found in Sergeev et al. 2011) and $FWHM(2001) \sim 12000 \text{km/s}$ for 3C390.3 from 1995 to 2000. It is clear that based on the measured line width (FWHM) and the size of BLR, we have $\frac{R_{BLR,2001}}{R_{BLR,2004}} \sim 3.8 \gg (\frac{FWHM(2004)}{FWHM(2001)})^2 \sim 0.5$, which indicates the measured line width (FWHM) varying does not obey the virialization assumption. In other words, in one long-term observed period, the effects of accretion disk physical parameter varying should be important, especially on the line profile varying, so that the measured line width (FWHM) can not accurately trace the kepler velocity of broad line clouds for long-term spectra.

In order to more clearly show our point: the positive correlation between the line width and the line flux is not fake, some evidence to the contrary is shown as follows. If we accept that the positive correlation shown in Figure 3 was fake for 3C390.3 and the common negative correlation could be applied for the double-peaked emitters, i.e., both the empirical relation $L \sim^{0.5} \propto R_{BLR}$ for time-varying size of BLR and applying peak separation (V_p) to replace the second moment were available for 3C390.3, we will have $L \times V_p^4 = constant$, under the virialization assumption. For the spectra of 3C390.3 in Shapovalova et al. (2001), the line luminosity ratio of maximum $L(H\beta)$ to minimum $L(H\beta)$ is about $\frac{L(max)}{L(min)} \sim 1.75$, however, the forth power of the line width ratio of minimum V_p to maximum V_p is about $(\frac{V_p(min)}{V_p(max)})^4 \sim (\frac{8000 \text{km/s}}{14000 \text{km/s}})^4 \sim 0.11$, which is against the expected result $\frac{L(max)}{L(min)} = (\frac{V_p(min)}{V_p(max)})^4$. Similarly, for NGC1097 in Schimoia et al. (2012) and Storchi-Bergmann et al. (2003), the line luminosity ratio of maximum $L(\alpha)$ to minimum $L(H\alpha)$ is about $\frac{L(max)}{L(min)} \sim 3.7$, however, the forth power of the line width ratio of minimum V_p to maximum V_p is about $(\frac{V_p(min)}{V_p(max)})^4 \sim (\frac{6000 \text{km/s}}{10000 \text{km/s}})^4 \sim 0.13$. Similar results can be found for the double-peaked emitters discussed in Lewis et al. (2010): the parameter $(\frac{V_p(min)}{V_p(max)})^4$ is much different from the parameter $\frac{L(max)}{L(min)}$, $(\frac{V_p(min)}{V_p(max)})^4 \sim 0.16$ and $\frac{L(max)}{L(min)} \sim 1.4$ for 3C59, $(\frac{V_p(min)}{V_p(max)})^4 \sim 0.06$ and $\frac{L(max)}{L(min)} \sim 2.2$ for IE0450.3, $(\frac{V_p(min)}{V_p(max)})^4 \sim 0.15$ and $\frac{L(max)}{L(min)} \sim 2.5$ for Pictor A, $(\frac{V_p(min)}{V_p(max)})^4 \sim 0.18$ and $\frac{L(max)}{L(min)} \sim 1.7$ for CBS74, $(\frac{V_p(min)}{V_p(max)})^4 \sim 0.31$ and $\frac{L(max)}{L(min)} \sim 2.1$ for PKS0921, $(\frac{V_p(min)}{V_p(max)})^4 \sim 0.53$ and $\frac{L(max)}{L(min)} \sim 1.8$ for PKS1020, $(\frac{V_p(min)}{V_p(max)})^4 \sim 0.27$ and $\frac{L(max)}{L(min)} \sim 2.5$ for PKS1739. The results re-confirm that for long-term observed double-peaked broad lines, the parameter of the peak separation is not one good substitute to trace the kepler velocity of the broad line clouds, and clearly indicates the correlation shown in Figure 3 is definitely different from the previous reported results about the peak separation in the literature.

The results above indicate that for double-peaked emitters, it should be one good choice to check the virialization assumption (the correlation of line parameters) by one sample of short-term observed spectra rather than by one sample of long-term observed spectra, in order to ignore the effects of physical disk parameters varying.

3.4 Indicator for Double-Peaked Emitters

Finally, we consider the question: whether the positive correlation of line parameters could be common for all double-peaked emitters, if the effects of BLR physical parameter varying could be clearly considered?

The most important starting point for the positive correlation is that the central ionizing continuum emission is coming from one point-like source, so that there are different arriving times of ionizing photos in different parts of disk-like BLRs of double-peaked emitters. However, as discussed in the literature, one 'external' ionizing source should be necessary for some double-peaked emitters (Chen et al. 1989, Eracleous & Halpern 1994, 2003, Luo et al. 2009, Strateva et al. 2003, 2006, 2008, Wu et al. 2008), due to the 'energy budget' problem: the total double-peaked broad line flux likely exceeds the viscous energy that can be extracted locally from the accretion disk. If the extended size of the 'external' ionizing source is large enough to cover the disk-like BLRs of double-peaked emitters, the expected different time delays for different parts of BLRs should be not so apparent, and then no apparent positive correlation between the line width and the line flux of broad double-peaked lines could be found.

Commonly, parameter $L(H\alpha)/W_d > 0.2$ (ratio of the double-peaked broad $H\alpha$ luminosity to the viscous power output of the line-emitting portion of the accretion disk) is used to determine existence of one 'external' ionizing source (Collin-Souffrin 1987, Dumont & Collin-Souffrin 1990, Strateva et al. 2008, Williams 1980). For 3C390.3, Eracleous & Halpern (2003, 1994) have shown that the parameter $L(H\alpha)/W_d$ is about $3.5 \times 10^{42} \text{erg/s} / 1.6 \times 10^{43} \text{erg/s} \sim 0.22$ with energy transfer efficiency $\eta \sim 0.01$ being accepted. Here the used $L(H\alpha)$ and W_d are the updated values listed in Eracleous & Halpern (2003). However, we should note that the energy transfer efficiency is much larger than 0.01 for 3C390.3. Based on the empirical relation shown in Davis & Laor (2011) and the more recent black hole mass of 3C390.3 in Dietrich et al. (2012, $M_{BH} \sim 10^9 M_\odot$), the energy transfer efficiency for 3C390.3 is about $\eta \sim 0.089 \times (M_{BH,8})^{0.52} \sim 0.29$. So that the parameter of $L(H\alpha)/W_d$ is about $L(H\alpha)/W_d \sim 0.0075$, which is much smaller than the limited value of $L(H\alpha)/W_d \sim 0.2$. So that, it is not necessary for one 'external' ionizing source for the double-peaked emitter 3C390.3. Furthermore, through the reverberation mapping technique (Blandford & McKee 1982, Peterson 1993), the UV emission region is within 5 light-days (Dietrich et al. 1998), which is much smaller than the size of BLR ($R_{BLR} \sim 20 \text{light} - \text{days}$ in Peterson et al. (2004) (certainly, much smaller than the size of BLR shown in Dietrich et al. 2012, Popovic et al. 2011, Sergeev et al. 2011 and Shapovalova et al. 2001). So that the time delays for different parts of the BLR of 3C390.3 are apparent, and one positive correlation shown in Figure 3 can be expected.

So far, It is still not clear about the structures of the probable needed 'external' ionizing source: external ionizing photos coming from an elevated structure in central region of accretion disk (standard RIAF, Cao 2005, Manmoto 2000), or ionizing photos coming from scattering ionizing photons radiated from the inner accretion disk region (Cao & Wang 2006), or other unknown structures. Before to confirm the structures of the 'external' ionizing source, it is very hard

to give one final conclusion that all double-peaked emitters show one positive correlation between line width and line flux for short-term observed spectra. However, after the corrections of the effects of disk physical parameters varying, once one positive correlation between the line width and the line flux can be confirmed for one broad line, it is extremely possible that the broad line comes from central accretion disk.

3.5 Conclusions

The final conclusions are as follows.

- Under the Virialization assumption and the commonly accepted empirical relation $R_{BLR} \propto L^{\sim 0.5}$, there should be one strong negative correlation between the line width and the line flux of broad lines for multi-observed spectra of broad line AGN: $L \times \sigma^4 = \text{constant}$. The negative correlation can be confirmed for some mapped objects, such as the results shown in Figure 5 for NGC5548.

- Based on the public spectra of 3C390.3 from the AG-NWATCH project, the correlation between the line width (second moment) and the line flux of the double-peaked broad $H\alpha$ is checked. However, one unexpected reliable positive correlation is confirmed and shown in Figure 3, which indicates there are different structures of BLR for the double-peaked emitter 3C390.3 and normal broad line AGN.

- In the context of the theoretical accretion disk model for double-peaked emitters, the unexpected positive correlation between the line width and the line flux can be naturally explained, due to the different time delays for the different parts of the disk-like BLRs of 3C390.3 in one short period.

- The Virialization assumption is further checked for the double-peaked emitter 3C390.3, $R_{BLR} \times \sigma^2 = \text{constant}$. Then, we find that the virialization assumption is still available for 3C390.3, however, the time-varying size of BLR in one period can not be expected through the empirical relation of $R_{BLR} \propto L^{\sim 0.5}$. For the double-peaked emitter 3C390.3, stronger continuum emission leads to smaller (not larger) flux-weighted size of BLR in one moment.

- Furthermore, we have shown that in the context of the accretion disk model, there are important effects on the correlation of the line parameters from the physical disk parameters varying (such as the accretion disk precession). That is why there are different conclusions in the literature about the correlation between the peak separation and the line flux for long-term observed double-peaked broad lines. Moreover, it should be better to check the correlation of line parameters of double-peaked broad line through short-term observed spectra, in order to ignore the effects from physical disk parameters varying.

- Finally, the correlation between the line width and the line flux is checked for the other double-peaked emitters. However, due to the probable 'external' ionizing source with so far unclear structures, it is hard to confirm that the positive correlation between the line width and the line flux of double-peaked broad lines can be found for all the double-peaked emitters. However, one strong positive correlation between the line width and the line flux of one broad line should strongly indicate accretion disk origination for the broad line.

ACKNOWLEDGMENTS

Zhang X. G. gratefully acknowledge the anonymous referee for giving us constructive comments and suggestions to greatly improve our paper. ZXG gratefully acknowledges the finance support from the Chinese grant NSFC-11003043, and thanks the project of AGNWATCH (<http://www.astronomy.ohio-state.edu/~agnwatch/>) to make us conveniently collect the spectra of 3C390.3 and NGC5548.

REFERENCES

- Bachev, R., 1999, *A&A*, 348, 71
 Barth A. J., Nguyen M. L., Malkan M. A., Filippenko A. V., Li W. D., et al., 2011, *ApJ*, 732, 121
 Begelman M. C., Blandford R. D. & Rees M. J., 1980, *Nature*, 287, 307
 Bennert N., Auger M. W., Treu T., Woo J.-H., Malkan M. A., 2011, *ApJ*, 726, 59
 Bentz M. C., Peterson B. M., Pogge R. W., Vestergaard M., Onken C. A., 2006, *ApJ*, 644, 133
 Bentz M. C., Denney K. D., Cackett E. M., Dietrich M., Fogel J. K. J., et al., 2007, *ApJ*, 662, 205
 Bentz M. C., Walsh J. L., Barth A. J., Baliber N., Bennert V. N., et al., 2009, *ApJ*, 705, 199
 Bentz M. C., Walsh J. L., Barth A. J., Yoshii Y., Woo J. H., et al., 2010, *ApJ*, 716, 993
 Blandford R. D. & McKee C. F., 1982, *ApJ*, 255, 419
 Boroson T. A. & Lauer T. R., 2009, *Nature*, 458, 53
 Burbidge E. M. & Burbidge G. R., 1971, *ApJ*, 163, L21
 Cao X. W., 2005, *ApJ*, 631, L101
 Cao X. W. & Wang T. G., 2006, *ApJ*, 652, 112
 Chen K. Y. & Halpern J. P., 1989, *ApJ*, 344, 115
 Chen K. Y., Halpern J. P. & Filippenko A. V., 1989, *ApJ*, 339, 742
 Chornock R., Bloom J. S., Cenko S. B., Filippenko A. V., Silverman J. M., Hicks M. D., Lawrence K. J., Mendez A. J., Rafelski M., Wolfe, A. M., 2010, *ApJ*, 709, 39
 Collin-Souffrin S. 1987, *A&A*, 179, 60
 Collin S., Kawaguchi T., Peterson B. M., Vestergaard M., 2006, *A&A*, 456, 75
 Davis S. W. & Laor A., 2011, *ApJ*, 728, 98
 Denney K. D., Bentz M. C., Peterson B. M., Pogge R. W., Cackett E. M., et al., 2006, *ApJ*, 653, 152
 Denney K. D., Peterson B. M., Pogge R. W., Adair A., Atlee D. W., et al., 2009, *ApJ*, 704, 80
 Denney K. D., Peterson B. M., Pogge R. W., Adair A., Atlee D. W., et al., 2010, *ApJ*, 721, 715
 Dietrich, M., Kollatschny, W., Peterson, B. M., Bechtold, J., Bertram R., et al., 1993, *ApJ*, 408, 416
 Dietrich M., Peterson B. M., Albrecht P., Altmann M., Barth A. J., et al., 1998, *ApJS*, 115, 185
 Dietrich M., Peterson B. M., Grier C. J., Bentz M. C., Eastman J., et al., 2012, *ApJ*, 757, 53D
 Down E. J., Rawlings S., Sivia D. S., Baker J. C., 2010, *MNRAS*, 401, 633
 Dumont A. M. & Collin-Souffrin S. 1990, *A&A*, 229, 313
 Eracleous M. & Halpern J. P., 1994, *ApJS*, 90, 1
 Eracleous M., Livio M., Halpern J. P., Storchi-Bergmann T., 1995, *ApJ*, 438, 610
 Eracleous M., Halpern J. P., Gilbert A. M., Newman J. A., Filippenko A. V., 1997, *ApJ*, 490, 216
 Eracleous M. & Halpern J. P., 2003, *ApJ*, 599, 886
 Flohic H. M. L. G. & Eracleous M., 2008, *ApJ*, 686, 138
 Fromerth M. J. & Melia F., 2000, *ApJ*, 533, 172
 Gaskell C. M., 1988, *ApJ*, 325, 114
 Gaskell M., 1996, *ApJ*, 464, 107
 Gaskell C. M., 2010, *Nature*, 463, 1
 Gezari S., Halpern J. P., Eracleous M., 2007, *ApJ*, 169, 167
 Greene J. E. & Ho L. C., 2004, *ApJ*, 610, 722
 Greene J. E. & Ho L. C., 2005, *ApJ*, 630, 122
 Greene J. E., Hood C. E., Barth A. J., Bennert V. N., Bentz M. C., et al., 2010, *ApJ*, 723, 409
 Hartnoll S. A. & Blackman E. G., 2000, *MNRAS*, 317, 880
 Hartnoll S. A. & Blackman E. G., 2002, *MNRAS*, 332, L1
 Karas V., Martocchia A. & Subr L., 2001, *PASJ*, 53, 189
 Kaspi S., Smith P. S., Maoz D., Netzer H., Jannuzi B. T., 1996, *ApJL*, 471, 75
 Kaspi S., Smith P. S., Netzer H., Maoz D., Jannuzi B. T., Giveon U., 2000, *ApJ*, 533, 631
 Kaspi S., Maoz D., Netzer H., Peterson B. M., Vestergaard M., Jannuzi B. T., 2005, *ApJ*, 629, 61
 Kaspi S., Brandt W. N., Maoz D., Netzer H., Schneider D. P., Shemmer O., 2007, *ApJ*, 659, 997
 Kelly B. C. & Bechtold J., 2007, *ApJS*, 168, 1
 Kollatschny W. & Zetzl M., 2011, *Nature*, 470, 366
 Korista K. T., Alloin D., Barr P., Clavel J., Cohen R. D., et al., 1995, *ApJS*, 97, 285
 Krause M., Burkert A., Schartmann M., 2011, *MNRAS*, 411, 550
 Lauer T. R. & Boroson T. A. 2009, *ApJ*, 703, 930
 Lewis K. T., Eracleous M., Storchi-Bergmann T., 2010, *ApJS*, 187, 416
 Livio M. & Xu C., 1997, *ApJ*, 478, L63
 Luo B., Brandt W. N., Silverman J. D., Strateva I. V., Bauer F. E., et al., 2009, *ApJ*, 695, 1227
 Marziani P., Sulentic J. W., Zamanov R., Calvani M., Dultzin-Hacyan D., Bachev R., Zwitter T., 2003, *ApJS*, 145, 199
 Manmoto T., 2000, *ApJ*, 534, 734
 Netzer H. & Marziani P., 2010, *ApJ*, 724, 318
 Oke J. B., IN: Superluminal radio sources; Proceedings of the Workshop, Pasadena, CA, Oct. 28-30, 1986 (A88-39751 16-90). Cambridge and New York, Cambridge University Press, 1987, p. 267-272.
 Onken C. A., Ferrarese L., Merritt D., Peterson B. M., Pogge R. W., Vestergaard M., Wandel A., 2004, *ApJ*, 615, 645
 Park D., Woo J. H., Treu T., Barth A. J., Bentz M. C., et al., 2012, *ApJ*, 747, 30
 Perez E., Penston M. V., Tadhunter C., Mediavilla E., Moles M., 1988, *MNRAS*, 230, 353
 Peterson B. M., Wanders I., Horne K., Collier S., 1998, *PASP*, 110, 660
 Peterson B. M. & Wandel A., 1999, *ApJ*, 521, L95
 Peterson B. M., Balonek T. J., Barker E. S., Bechtold J., Bertram R., et al., 1991, *ApJ*, 368, 119
 Peterson B. M., Alloin D., Axon D., Balonek T. J., Bertram R., et al., 1992, *ApJ*, 392, 470
 Peterson, B. M., 1993, *PASP*, 105, 247
 Peterson B. M., Berlind P., Bertram R., Bochkarev N. G., Bond D., et al., 1994, *ApJ*, 425, 622
 Peterson B. M., Barth A. J., Berlind P., Bertram R., Bischoff K., et al., 1999, *ApJ*, 510, 659
 Peterson B. M., Berlind P., Bertram R., Bischoff K., Bochkarev N. G., et al., 2002, *ApJ*, 581, 197
 Peterson B. M., Ferrarese L., Gilbert K. M., Kaspi S., et al., 2004, *ApJ*, 613, 682
 Peterson B. M., 2010, Co-Evolution of Central Black Holes and Galaxies, Proceedings of the International Astronomical Union, IAU Symposium, Volume 267, p. 151-160
 Popovic L. C., Shapovalova A. I., Chavushyan V. H., Ilic D., Burenkov A. N., Mercado A., Bochkarev N. G., 2008, *PASJ*, 60, 1
 Popovic L. C., Shapovalova A. I., Ilic D., Kovacevic A., Kol-

- latschny W., Burenkov A. N., Chavushyan V. H., Bochkarev N. G., Leon-Tavares J., 2011, *A&A*, 528, 130
- Press W. H., Teukolsky S. A., Vetterling W. T., Flannery B. P., 1992, 'Numerical Recipes in Fortran 77', Second Edition, published by the Press Syndicate of the University of Cambridge, ISBN 0-521-43064-X, P340
- Rafiee A., & Hall P. B., 2011, *ApJS*, 194, 42
- Schimoia J. S., Storchi-Bergmann T., Nemmwn R. S., Winge C., Eracleous M., 2012, *ApJ*, 748, 145
- Sergeev S. G., Doroshenko V. T., Dzyuba S. A., Peterson B. M., Pogge R. W., Pronik V. I., 2007, *ApJ*, 668, 708
- Sergeev S. G., Kilmanov S. A., Doroshenko V. T., Efimov Y. S., Nazarov S. V., Pronik V. I., 2011, *MNRAS*, 410, 1877
- Shapovalova A. I., Burenkov A. N., Carrasco L., Chavushyan V. H., Doroshenko V. T., et al., 2001, *A&A*, 376, 775
- Shapovalova A. I., Doroshenko V. T., Bochkarev N. G., Burenkov A. N., Carrasco L., et al., 2004, 422, 925
- Shapovalova A. I., Popovic L. C., Burenkov A. N., Chavushyan V. H., Ilic D., et al., 2010, *A&A*, 517, 42
- Shen Y. & Liu X., 2012, *ApJ*, 753, 125
- Sluse D., Schmidt R., Courbin F., Hutsemekers D., Meylan G., Eigenbrod A., Anguita T., Agol E., Wambsganss J., 2011, *A&A*, 528, 100
- Sulentic J. W., Marziani P., Dultzin-Hacyan D., 2000, *ARA&A*, 38, 521
- Storchi-Bergmann T., Nemmen da S. R., Eracleous M., Halpern J. P., Wilson A. S., Filippenko A. V., Ruiz M. T., Smith R. C., Nagar N. M., 1997, *ApJ*, 489, 8
- Strateva I. V., Strauss M. A., Hao L., Schlegel D. J., Hall P. B., et al., 2003, *AJ*, 126, 1720
- Strateva I. V., Brandt W. N., Eracleous M., Schneider D. P., Chartas, G. 2006, *ApJ*, 651, 749
- Strateva I. V., Brandt W. N., Eracleous M., Garmire G., 2008, *ApJ*, 687, 869
- Tran H. D., 2010, *ApJ*, 711, 1174
- van Groningen, E. & Wanders, I., 1992, *PASP*, 104, 700
- Veilleux S. & Zheng W., 1991, *ApJ*, 377, 89
- Vestergaard M., 2002, *ApJ*, 571, 733
- Wandel A., Peterson B. M., & Malkan M. A., 1999, *ApJ*, 526, 579
- Wanders I. & Peterson B. M., 1996, *ApJ*, 466, 174
- Wang T. G., & Zhang X. G., 2003, *MNRAS*, 340, 793
- Williams R. E., 1980, *ApJ*, 235, 939
- Wu S. M., Wang T. G., Dong X. B., 2008, *MNRAS*, 389, 213
- Wu X. B., Wang R., Kong M. Z., Liu F.K., Han J. L., 2004, *A&A*, 424, 793
- Zhang X. G., Dultzin D., Wang T. G., 2007, *MNRAS*, 377, 1215
- Zhang X. G., 2011a, *MNRAS*, 416, 2857
- Zhang X. G., 2011b, *ApJ*, 741, 104
- Zheng W., Sulentic J. W., Binette L., 1990, *ApJ*, 365, 115
- Zheng W., Veilleux S., Grandi S. A., 1991, *ApJ*, 381, 418

Table 1. Line Parameters of the double-peaked broad H α of 3C390.3

id	f_0	f_1	σ	R	id	f_0	f_1	σ	R
49517fe	632.6±14.8	1033.1±24.2	93.18±1.97	0.592	49871ce	680.0±21.2	1115.7±34.8	97.31±2.25	0.657
49596dr	587.5±17.5	950.7±28.4	93.44±1.32	0.546	49871fe	736.5±19.9	1144.9±31.0	99.63±1.74	0.641
49599dr	629.9±16.8	956.7±25.5	91.56±1.33	0.561	49872dr	671.6±19.0	1082.5±30.7	95.81±2.18	0.659
49622dr	713.7±22.5	990.5±31.2	91.06±2.82	0.575	49873ce	694.2±20.8	1080.3±32.3	97.55±1.98	0.643
49638dr	756.8±20.5	970.0±26.2	94.11±2.39	0.584	49874ce	724.7±22.2	1056.2±32.4	97.76±2.51	0.649
49652dr	593.9±13.2	984.8±21.8	89.97±2.81	0.578	49890ce	676.4±19.6	1116.6±32.4	97.92±1.95	0.613
49664dr	667.4±19.0	975.6±27.8	93.51±1.79	0.567	49890dr	694.8±21.0	1101.5±33.3	95.18±3.37	0.642
49743dr	630.6±19.2	964.7±29.4	92.67±2.75	0.613	49891ce	689.1±20.6	1057.4±31.7	98.44±2.26	0.634
49753dr	574.3±16.8	1009.2±29.6	91.39±2.79	0.632	49892ce	648.6±18.3	1066.5±30.1	96.89±2.23	0.586
49770dr	582.6±17.8	973.3±29.7	89.46±2.88	0.581	49893ce	529.6±16.7	1042.8±32.9	95.98±2.09	0.701
49772dr	674.7±19.8	979.1±28.8	94.10±2.08	0.629	49894ce	938.1±28.7	1087.9±33.2	98.68±2.06	0.682
49783dr	626.6±17.9	972.0±27.8	93.77±1.48	0.611	49895ce	844.7±26.3	1028.9±32.1	98.21±2.95	0.633
49844dr	663.5±17.3	1065.1±27.7	93.47±2.85	0.584	49897ce	572.0±16.2	1053.2±29.8	96.29±2.87	0.617
49860ce	681.9±20.6	1067.9±32.3	98.31±2.02	0.627	49899ce	777.8±23.7	1078.7±32.8	100.44±1.71	0.622
49861be	836.0±25.8	1052.6±32.5	95.91±1.92	0.604	49901dr	803.1±22.6	1042.3±29.3	94.93±1.66	0.617
49861ce	696.9±21.1	1074.3±32.6	98.06±2.21	0.614	49905be	909.2±24.8	1069.8±29.2	95.73±1.83	0.623
49861dr	602.0±17.5	1075.2±31.2	95.24±2.32	0.609	49923be	891.6±22.6	1053.5±26.7	97.21±1.78	0.637
49862ce	634.2±19.1	1044.7±31.5	97.87±2.04	0.627	49924ce	748.6±21.4	1080.6±30.9	99.44±2.04	0.669
49863ce	666.5±20.2	1066.8±32.3	98.45±2.46	0.631	49930be	911.4±24.6	1039.5±28.1	96.89±1.94	0.633
49864ce	886.7±27.3	1056.4±32.6	97.67±2.44	0.674	49934dr	736.6±21.8	1038.6±30.7	96.31±1.84	0.643
49865ce	875.3±27.2	1038.5±32.2	98.19±2.16	0.628	49935dr	713.1±20.8	1062.1±31.0	96.79±2.41	0.633
49866ce	761.9±21.6	1045.1±29.7	98.05±1.99	0.645	49952dr	652.6±20.1	1073.4±33.1	96.66±1.64	0.648
49867ce	730.9±20.6	1034.3±29.1	95.54±2.15	0.638	49953be	757.5±19.1	1059.5±26.7	96.94±1.91	0.665
49868ak	1006.2±27.6	1072.6±29.5	96.08±1.28	0.619	49979dr	769.9±24.3	1097.9±34.7	93.91±2.08	0.658
49868bk	1032.4±30.2	1099.1±32.1	95.21±1.33	0.635	49980dr	711.4±20.8	1130.4±33.1	95.04±2.11	0.628
49868ck	1095.8±31.6	1051.1±30.3	95.85±1.18	0.621	49981ce	811.9±24.8	1159.0±35.5	100.54±2.22	0.682
49868dk	1021.6±22.9	1100.3±24.6	95.83±2.39	0.617	49984ce	654.5±20.7	1107.2±35.1	97.62±2.09	0.692
49869ak	1111.5±27.9	1051.3±26.3	96.56±1.25	0.643	49985ce	526.3±16.1	1153.4±35.4	99.81±2.69	0.681
49869bk	828.2±21.0	1092.6±27.7	96.25±1.08	0.634	49986be	824.8±24.7	1096.9±32.9	96.95±1.11	0.682
49869ce	671.2±19.6	1042.6±30.5	98.57±1.98	0.628	49988ac	1316.6±40.1	1114.5±34.0	99.44±2.66	0.715
49869ck	926.6±26.8	1108.9±32.1	95.52±1.24	0.633	50007be	963.7±31.1	1146.1±37.0	96.57±1.94	0.663
49869dk	987.1±22.2	1044.6±23.5	95.55±1.21	0.612	50051be	965.1±31.9	1271.9±42.1	96.21±1.03	0.619
49870ce	661.2±18.5	1041.9±29.2	98.05±2.95	0.615	50068be	1116.9±34.8	1245.5±38.8	94.59±1.91	0.592
49870dr	738.8±21.5	1130.7±32.9	91.73±2.26	0.644					

Notice: The columns of 'id' show ids of the spectra, including observational dates (JD-2400000) and corresponding instrument codes as listed in Dietrich et al. (1998). The columns of ' f_0 ' give the line flux of the double-peaked broad H α directly measured from the observed spectra, in unit of 10^{-15} erg/s/cm², the uncertainty of f_0 is calculated by $f_0/f_1 \times f_{1,err}$. The columns of ' f_1 ' show the accurate flux of the H α collected from the AGNWATCH project, after necessary corrections. The columns of ' σ ' give the measured line widths of the double-peaked broad H α , in unit of Å. The columns of ' R ' show the flux ratio of the broad H α from the inner half part of the disk-like BLR to the total flux of the broad H α as discussed in Section 3.1.

Table 2. Line Parameters of the broad H β of mapped Seyfert 1 NGC5548

id	f	σ									
7512m	71.4 \pm 4.2	35.66 \pm 0.26	7900a	71.4 \pm 4.2	34.31 \pm 0.29	8513a	51.1 \pm 4.2	36.03 \pm 0.29	8992a	67.3 \pm 4.7	35.88 \pm 0.25
7517a	71.7 \pm 4.3	35.47 \pm 0.31	7912h	63.2 \pm 4.5	35.59 \pm 0.30	8514a	48.3 \pm 4.6	35.51 \pm 0.45	9000a	71.6 \pm 4.9	35.76 \pm 0.24
7534a	73.2 \pm 4.3	34.14 \pm 0.35	7915a	63.7 \pm 4.3	35.40 \pm 0.27	8516a	51.0 \pm 4.5	35.98 \pm 0.39	9008a	69.2 \pm 4.3	35.82 \pm 0.20
7535a	73.1 \pm 4.3	34.68 \pm 0.29	7929a	53.7 \pm 4.2	36.32 \pm 0.43	8531h	57.0 \pm 4.3	36.74 \pm 0.41	9010w	75.7 \pm 4.6	35.97 \pm 0.35
7549m	78.2 \pm 4.3	31.86 \pm 0.25	7949a	52.2 \pm 4.1	36.46 \pm 0.44	8636a	61.6 \pm 4.9	37.45 \pm 0.61	9013a	70.4 \pm 4.3	36.20 \pm 0.21
7560a	77.5 \pm 4.5	33.88 \pm 0.34	7957a	43.8 \pm 4.1	37.76 \pm 0.43	8644a	64.1 \pm 4.8	37.71 \pm 0.37	9014w	76.4 \pm 4.6	36.53 \pm 0.34
7573a	78.2 \pm 4.2	34.25 \pm 0.26	7958a	43.9 \pm 4.1	37.87 \pm 0.43	8651a	62.4 \pm 4.8	37.11 \pm 0.64	9017h	68.7 \pm 4.6	36.50 \pm 0.35
7573m	77.0 \pm 4.2	32.96 \pm 0.21	7971a	39.8 \pm 4.2	38.30 \pm 0.37	8670a	58.1 \pm 4.6	37.04 \pm 0.48	9020a	66.5 \pm 5.0	36.05 \pm 0.25
7574m	76.4 \pm 4.5	33.59 \pm 0.27	7982a	35.4 \pm 4.1	38.92 \pm 0.54	8676a	61.4 \pm 4.3	37.56 \pm 0.38	9029a	66.0 \pm 4.7	36.03 \pm 0.29
7575m	76.9 \pm 4.2	33.53 \pm 0.24	7990a	34.7 \pm 4.1	38.22 \pm 0.26	8691a	51.2 \pm 4.2	37.77 \pm 0.38	9032h	67.4 \pm 4.8	36.75 \pm 0.23
7576m	74.3 \pm 4.2	32.79 \pm 0.22	7994a	37.8 \pm 4.2	38.73 \pm 0.40	8699a	45.1 \pm 4.3	37.53 \pm 0.45	9034w	71.3 \pm 4.7	36.38 \pm 0.29
7582a	69.5 \pm 4.2	34.74 \pm 0.31	8007a	44.3 \pm 4.2	38.85 \pm 0.40	8713a	33.2 \pm 4.3	38.51 \pm 0.58	9048a	62.0 \pm 4.7	36.05 \pm 0.25
7587m	72.6 \pm 4.5	34.32 \pm 0.42	8011h	45.1 \pm 4.3	38.63 \pm 0.39	8720a	24.9 \pm 4.2	38.46 \pm 0.54	9056a	65.1 \pm 4.8	37.01 \pm 0.25
7589m	70.5 \pm 4.6	34.04 \pm 0.28	8013a	44.9 \pm 4.2	38.06 \pm 0.27	8726a	23.7 \pm 4.2	39.65 \pm 0.61	9062a	70.2 \pm 4.5	36.69 \pm 0.30
7592m	71.4 \pm 4.6	33.50 \pm 0.21	8020a	49.5 \pm 4.2	38.09 \pm 0.41	8733a	21.3 \pm 4.2	38.89 \pm 0.64	9064a	68.8 \pm 4.6	36.02 \pm 0.23
7594m	62.5 \pm 4.2	34.00 \pm 0.33	8028a	52.5 \pm 4.1	37.75 \pm 0.26	8733h	23.0 \pm 4.2	39.04 \pm 0.56	9070w	73.5 \pm 4.5	36.38 \pm 0.27
7597m	63.7 \pm 4.2	33.58 \pm 0.24	8037a	55.5 \pm 4.2	38.02 \pm 0.35	8742a	20.8 \pm 4.2	40.25 \pm 0.81	9074w	71.3 \pm 4.4	36.42 \pm 0.92
7601m	64.8 \pm 4.2	34.10 \pm 0.21	8044a	59.3 \pm 4.2	37.66 \pm 0.28	8742w	22.3 \pm 4.1	37.12 \pm 1.13	9077w	73.2 \pm 4.5	37.05 \pm 0.34
7606m	57.9 \pm 4.2	31.52 \pm 0.22	8056h	60.0 \pm 4.2	37.83 \pm 0.30	8744w	23.0 \pm 4.1	40.82 \pm 0.80	9078m	67.3 \pm 4.3	36.60 \pm 0.27
7618a	74.0 \pm 5.1	34.54 \pm 0.31	8061a	61.1 \pm 4.1	37.24 \pm 0.22	8745w	23.6 \pm 4.1	39.09 \pm 0.76	9078w	73.0 \pm 4.4	36.57 \pm 0.27
7627a	77.5 \pm 5.0	33.64 \pm 0.41	8068a	58.7 \pm 4.2	37.30 \pm 0.26	8746w	22.2 \pm 4.1	40.99 \pm 0.60	9079a	65.7 \pm 4.7	36.24 \pm 0.29
7642a	84.9 \pm 4.8	33.04 \pm 0.15	8077a	50.9 \pm 4.1	36.88 \pm 0.24	8750a	22.0 \pm 4.1	39.71 \pm 0.60	9080m	67.1 \pm 4.3	36.88 \pm 0.32
7644m	78.1 \pm 4.2	32.49 \pm 0.23	8089h	45.7 \pm 4.4	38.14 \pm 0.42	8765h	26.3 \pm 4.1	41.01 \pm 0.37	9083m	65.5 \pm 4.2	36.67 \pm 0.33
7648m	83.5 \pm 4.3	32.70 \pm 0.16	8089m	42.8 \pm 4.3	37.34 \pm 0.42	8777w	28.2 \pm 4.1	40.22 \pm 0.59	9085a	64.5 \pm 4.3	36.56 \pm 0.31
7649a	90.5 \pm 4.6	32.95 \pm 0.21	8090a	44.7 \pm 4.1	37.52 \pm 0.28	8778w	27.3 \pm 4.1	38.87 \pm 0.58	9088w	66.7 \pm 4.6	36.83 \pm 0.36
7652m	88.0 \pm 4.2	33.30 \pm 0.22	8097a	44.1 \pm 4.1	38.39 \pm 0.36	8780a	29.4 \pm 4.1	40.04 \pm 0.54	9089w	66.0 \pm 4.5	36.86 \pm 0.31
7652m	88.8 \pm 4.2	33.31 \pm 0.23	8102h	46.2 \pm 4.1	39.25 \pm 0.36	8783h	30.2 \pm 4.1	39.31 \pm 0.46	9090a	58.8 \pm 4.4	36.59 \pm 0.34
7653a	91.7 \pm 4.4	32.94 \pm 0.27	8128a	60.3 \pm 4.1	38.63 \pm 0.37	8789a	37.8 \pm 4.3	38.26 \pm 0.41	9090h	61.5 \pm 4.4	37.03 \pm 0.27
7653a	94.6 \pm 4.3	33.08 \pm 0.26	8143a	52.9 \pm 4.2	38.97 \pm 0.33	8796a	36.8 \pm 4.3	41.38 \pm 0.51	9091h	60.5 \pm 4.4	36.93 \pm 0.29
7654a	87.5 \pm 4.3	32.61 \pm 0.19	8148a	51.7 \pm 4.2	38.82 \pm 0.45	8804a	31.2 \pm 4.1	38.81 \pm 0.35	9092h	59.8 \pm 4.3	37.21 \pm 0.24
7654a	90.0 \pm 4.2	32.78 \pm 0.25	8149a	52.1 \pm 4.1	39.33 \pm 0.31	8804w	34.8 \pm 4.1	39.50 \pm 0.51	9099a	55.7 \pm 4.4	36.99 \pm 0.23
7655a	93.1 \pm 4.8	33.69 \pm 0.23	8151a	49.8 \pm 4.2	39.10 \pm 0.41	8810h	28.9 \pm 4.1	38.45 \pm 0.46	9107a	56.9 \pm 4.5	36.15 \pm 0.28
7656m	88.2 \pm 4.2	33.91 \pm 0.22	8160a	49.4 \pm 4.2	39.08 \pm 0.31	8817a	28.7 \pm 4.3	41.21 \pm 0.63	9107h	59.6 \pm 4.7	36.44 \pm 0.29
7657a	90.4 \pm 4.5	33.06 \pm 0.18	8179a	56.2 \pm 4.4	38.52 \pm 0.42	8825a	27.3 \pm 4.1	39.09 \pm 0.44	9114a	63.3 \pm 4.5	35.41 \pm 0.30
7657a	92.4 \pm 4.4	33.57 \pm 0.28	8231a	64.3 \pm 4.2	37.08 \pm 0.26	8830w	28.7 \pm 4.1	38.55 \pm 0.46	9128a	65.5 \pm 4.5	35.54 \pm 0.24
7663m	92.1 \pm 4.6	33.06 \pm 0.17	8236a	64.2 \pm 4.3	36.61 \pm 0.23	8831a	26.9 \pm 4.1	38.37 \pm 0.47	9135a	67.8 \pm 4.5	36.07 \pm 0.20
7663m	91.3 \pm 5.0	33.62 \pm 0.26	8252a	68.6 \pm 4.3	35.77 \pm 0.15	8831w	30.6 \pm 4.1	38.75 \pm 0.36	9141w	69.7 \pm 4.4	37.65 \pm 0.32
7663m	95.1 \pm 4.8	33.35 \pm 0.22	8267a	69.3 \pm 4.5	34.90 \pm 0.19	8833w	33.0 \pm 4.1	39.24 \pm 0.51	9142a	66.2 \pm 4.7	36.08 \pm 0.82
7664m	90.1 \pm 4.4	33.45 \pm 0.29	8275a	68.6 \pm 4.3	35.03 \pm 0.21	8834w	32.1 \pm 4.1	38.40 \pm 0.44	9149a	62.1 \pm 4.5	35.76 \pm 0.21
7665m	89.7 \pm 4.2	33.18 \pm 0.21	8280a	68.3 \pm 4.3	35.06 \pm 0.26	8835w	34.0 \pm 4.1	38.73 \pm 0.44	9156a	63.9 \pm 4.4	36.97 \pm 0.25
7666m	88.5 \pm 4.2	33.38 \pm 0.18	8287a	69.5 \pm 4.3	35.19 \pm 0.18	8836w	33.4 \pm 4.1	38.76 \pm 0.46	9156w	63.8 \pm 4.4	36.68 \pm 0.34
7668m	88.1 \pm 4.2	33.94 \pm 0.24	8294a	67.7 \pm 5.0	34.79 \pm 0.32	8837h	29.9 \pm 4.1	38.58 \pm 0.36	9157w	63.3 \pm 4.3	37.02 \pm 0.34
7678a	86.7 \pm 4.3	33.86 \pm 0.29	8310a	65.3 \pm 4.3	35.15 \pm 0.27	8837w	32.0 \pm 4.1	38.62 \pm 0.48	9158w	60.0 \pm 4.2	36.32 \pm 0.33
7711a	78.6 \pm 4.5	35.04 \pm 0.39	8323a	71.3 \pm 4.4	35.82 \pm 0.28	8839a	30.3 \pm 4.2	39.19 \pm 0.38	9159w	60.9 \pm 4.2	37.08 \pm 0.25
7713m	68.6 \pm 4.1	34.41 \pm 0.25	8338a	72.4 \pm 4.3	34.78 \pm 0.21	8848a	34.7 \pm 4.3	37.35 \pm 0.41	9163a	57.3 \pm 4.3	36.52 \pm 0.22
7725a	84.6 \pm 4.6	35.43 \pm 0.38	8344a	72.6 \pm 4.6	36.24 \pm 0.24	8858h	39.5 \pm 4.1	36.63 \pm 0.29	9166h	59.0 \pm 4.4	36.99 \pm 0.24
7746m	71.1 \pm 4.4	36.53 \pm 0.38	8351a	72.0 \pm 4.2	35.81 \pm 0.31	8858w	46.0 \pm 4.2	38.02 \pm 0.29	9169a	57.8 \pm 4.2	36.35 \pm 0.23
7749m	60.5 \pm 4.1	35.74 \pm 0.26	8352a	69.4 \pm 4.3	35.25 \pm 0.30	8861w	49.0 \pm 4.2	38.60 \pm 0.39	9176a	60.2 \pm 4.3	36.38 \pm 0.25
7754m	66.0 \pm 4.1	35.68 \pm 0.38	8365a	58.1 \pm 4.2	36.05 \pm 0.33	8862a	42.6 \pm 4.3	37.25 \pm 0.36	9182h	63.3 \pm 4.2	36.29 \pm 0.35
7757m	64.1 \pm 4.5	35.58 \pm 0.34	8378a	57.2 \pm 4.3	37.18 \pm 0.41	8862w	45.7 \pm 4.2	36.25 \pm 0.24	9183a	63.1 \pm 4.4	36.91 \pm 0.23
7758m	60.2 \pm 4.3	36.72 \pm 0.40	8386a	57.4 \pm 4.5	37.07 \pm 0.35	8867h	42.9 \pm 4.3	38.21 \pm 0.35	9190a	64.6 \pm 4.5	36.64 \pm 0.22
7759m	60.7 \pm 4.1	35.71 \pm 0.34	8393a	58.4 \pm 4.2	36.99 \pm 0.35	8869a	41.0 \pm 4.5	37.55 \pm 0.42	9196h	66.9 \pm 4.4	36.49 \pm 0.37
7765m	58.2 \pm 4.1	35.49 \pm 0.33	8400a	59.1 \pm 4.3	36.94 \pm 0.27	8876a	45.4 \pm 4.3	37.92 \pm 0.35	9197a	64.8 \pm 4.5	36.25 \pm 0.24
7767m	59.1 \pm 4.1	36.10 \pm 0.27	8414a	48.7 \pm 4.2	36.77 \pm 0.38	8883a	44.8 \pm 4.5	37.53 \pm 0.32	9205a	66.2 \pm 4.3	37.18 \pm 0.32
7777h	66.3 \pm 4.6	36.02 \pm 0.30	8421a	43.8 \pm 4.2	34.96 \pm 0.28	8886h	43.8 \pm 4.3	37.64 \pm 0.32	9211a	63.1 \pm 4.5	36.78 \pm 0.23
7797h	78.3 \pm 4.9	35.24 \pm 0.36	8431a	49.4 \pm 4.4	36.19 \pm 0.38	8889a	45.6 \pm 4.5	37.08 \pm 0.35	9212h	65.6 \pm 4.8	37.59 \pm 0.26
7809h	80.0 \pm 4.7	34.46 \pm 0.25	8455a	58.8 \pm 4.2	36.11 \pm 0.31	8898a	49.2 \pm 4.3	38.17 \pm 0.25	9240a	58.7 \pm 4.5	38.15 \pm 0.23
7868a	77.5 \pm 4.4	35.77 \pm 0.27	8456a	58.2 \pm 4.2	36.55 \pm 0.40	8898h	46.2 \pm 4.4	37.18 \pm 0.37	9240h	60.5 \pm 4.7	38.48 \pm 0.25
7884a	79.1 \pm 4.2	34.55 \pm 0.25	8460a	53.5 \pm 4.2	35.69 \pm 0.41	8954a	57.6 \pm 4.8	37.06 \pm 0.32	9242h	60.2 \pm 4.6	38.13 \pm 0.30
7891a	80.0 \pm 4.3	35.00 \pm									

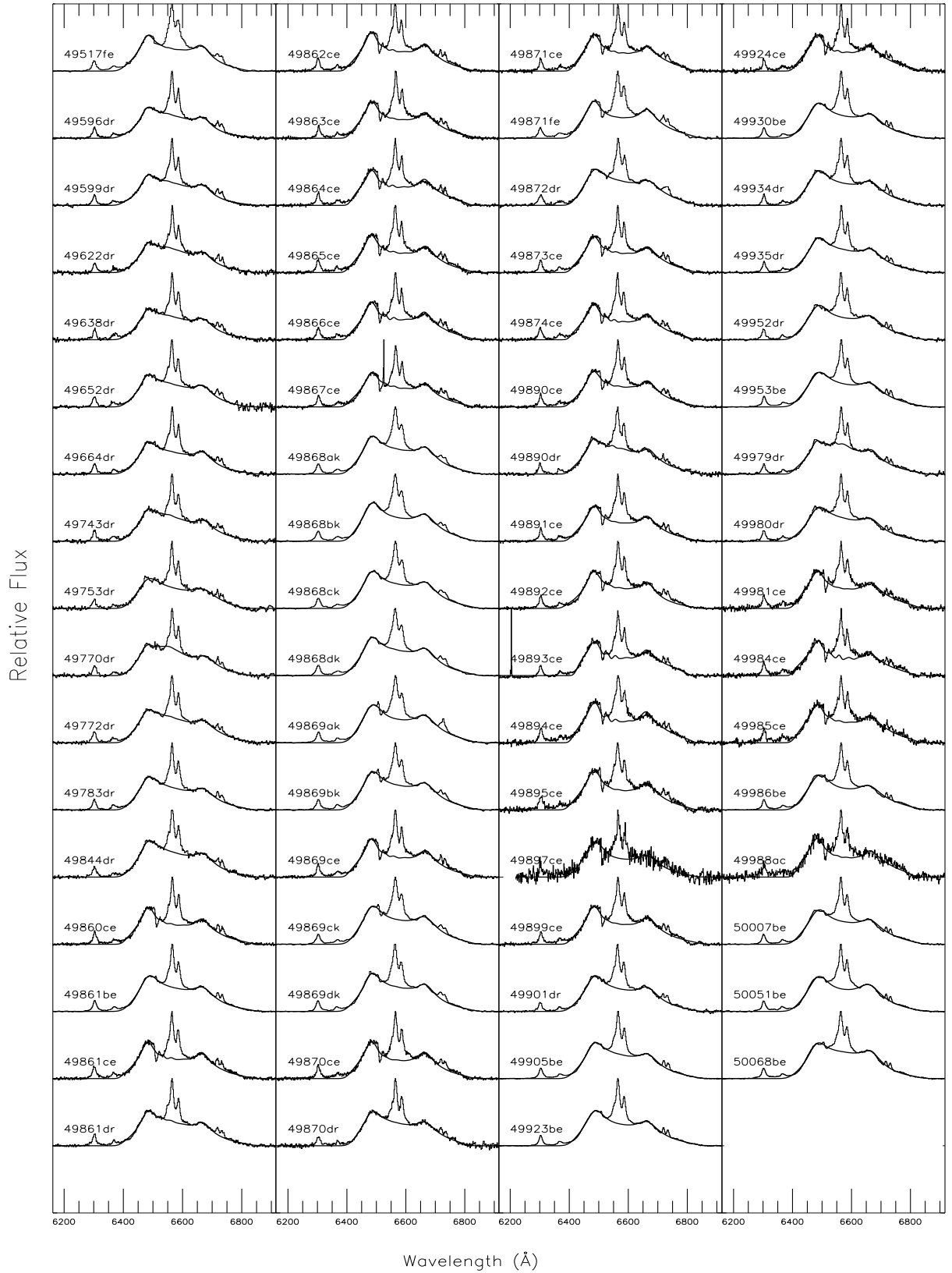


Figure 1. The best fitted results for the double-peaked broad $H\alpha$ of 3C390.3. Thin solid line represents the observed spectrum, thick solid line represents the best fitted results for the double-peaked broad component of $H\alpha$. The corresponding ID is marked for each spectrum.

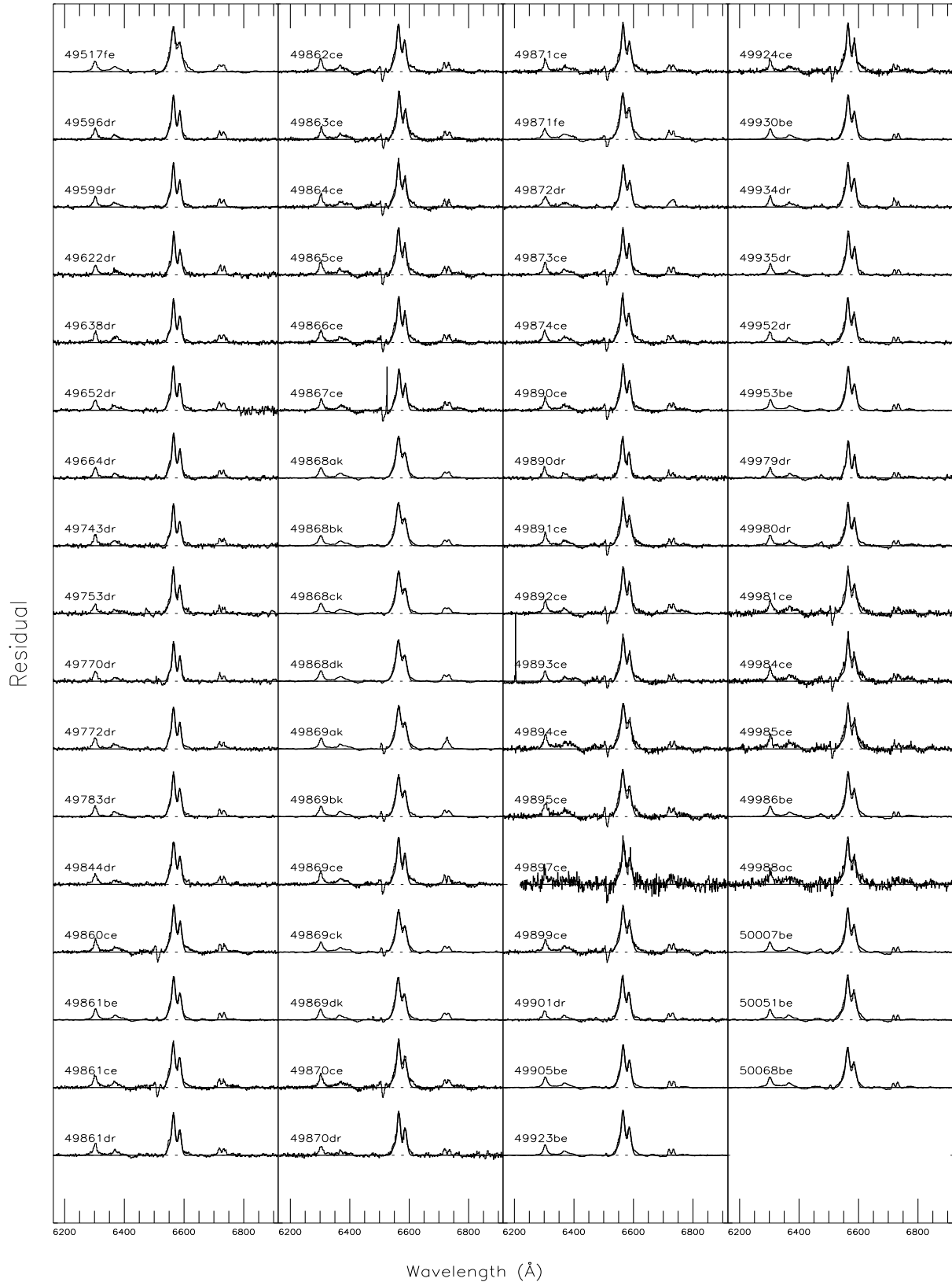


Figure 2. The residuals (observed spectrum minus the broad double-peaked component of H α) for the spectra shown in Figure 1. Thin solid line represents the residual. Thick solid line represents the best fitted results for the narrow H α and [N II] λ 6548, 6583 Å doublet by standard gaussian functions. The corresponding ID is marked for each spectrum.

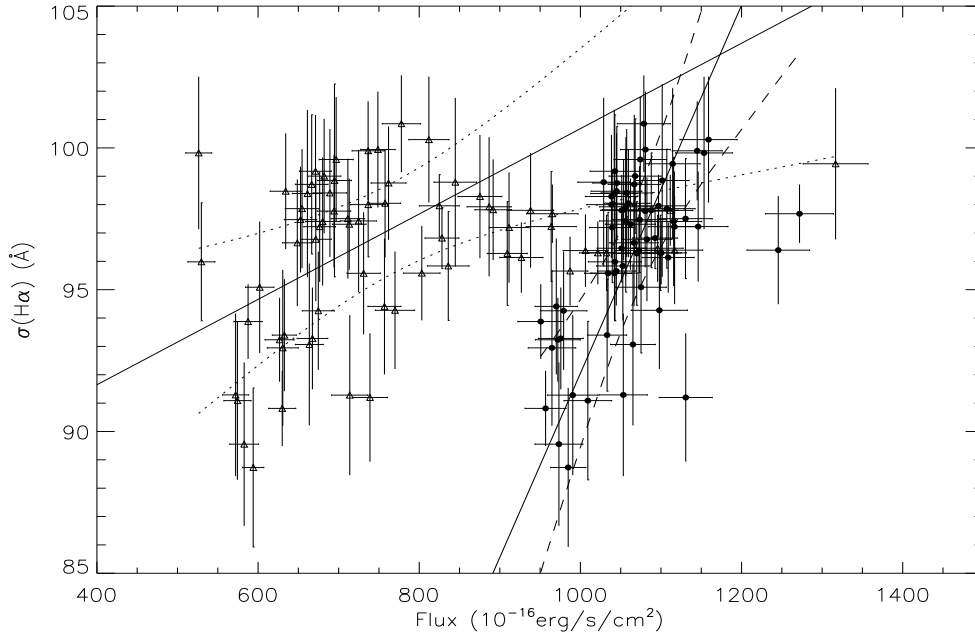


Figure 3. The correlation between the line with (second moment) and the line flux of the double-peaked broad H α of 3C390.3. Open triangles are for f_0 (no corrections for the different flux scales of different spectra) listed in table 1, solid circles are for f_1 collected from the AGNWATCH project. Thin solid line and dotted lines represent the best fitted results for the open triangles and the corresponding 99.95% confidence bands. Thick solid line and dashed lines represent the best fitted results for the solid circles and the corresponding 99.95% confidence bands.

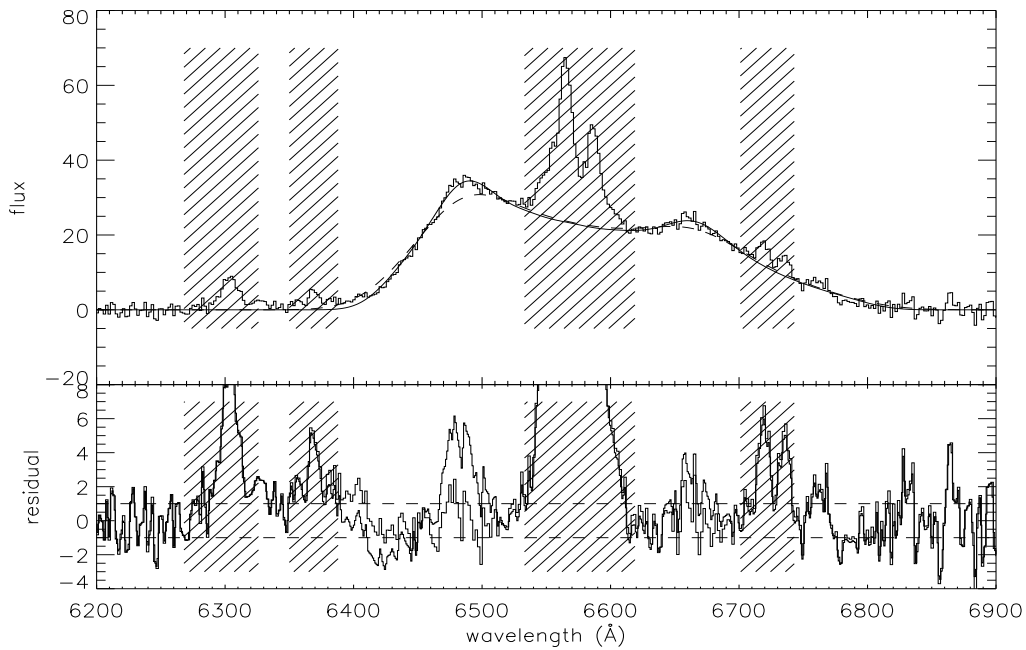


Figure 4. In top panel, thin solid line represents the observed spectrum of '49870dr', thick solid line represents the best fitted results, thick dashed line represents the being broadened double-peaked broad line profile with $\sigma_b = 1000\text{km/s}$. In bottom panel, the corresponding residuals are shown, thin line is for the best fitted results, solid thick line is for the being broadened results. In the two panels, shadow areas are the masked regions for the narrow lines.

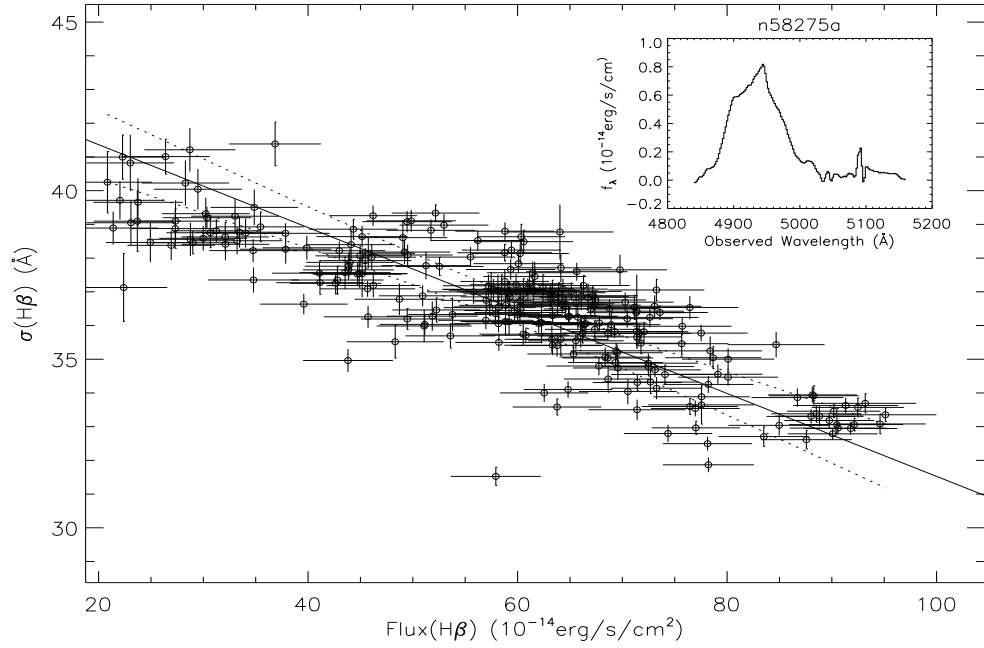


Figure 5. The correlation between the line width and the line flux of the broad H β of NGC5548. Solid line represents the best fitted results, dotted lines represent the corresponding 99.95% confidence bands. In top-right panel, one line profile of the pure broad H β is shown.

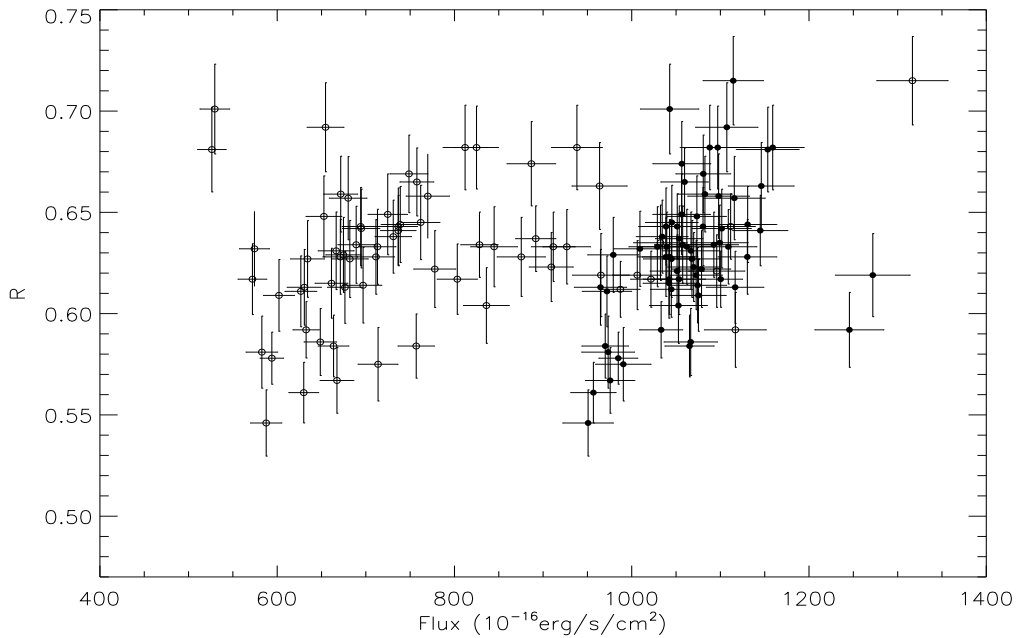


Figure 6. The correlation between the line flux of the double-peaked broad H α and the parameter of R . Open circles are for f_0 in Table 1 and solid circles are for f_1 in Table 1.